Project Description – Project Proposals

Frank A. Müller, Jena

Dynamic wetting of laser-induced periodic surface structures

Project Description

1 State of the art and preliminary work

Wettability

The wetting behavior of a solid surface depends on the surface energy γ of the liquid, the interfacial energy γ_{sv} between solid and vapor, and the interfacial energy γ_{sl} between solid and liquid (Figure 1a). The intrinsic contact angle θ of a smooth and inert surface can then be described by Young´s equation [You05]:

$$\cos\theta = \frac{\gamma_{sv}-\gamma_{sl}}{\gamma} \quad (1)$$

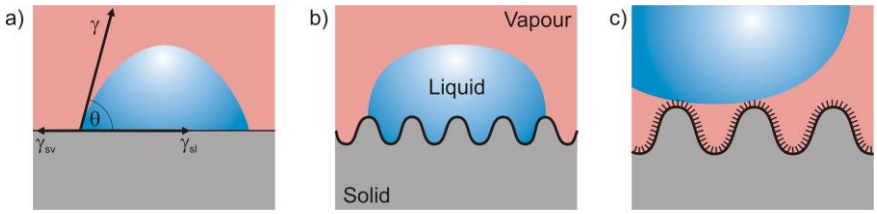

Figure 1: Wetting states: a) Young, b) Wenzel, and c) Cassie-Baxter.

By convention, surfaces with a contact angle $\theta < 90°$ are referred to as wetting, those with $\theta > 90°$ as non-wetting. In the case of liquid water, wetting and non-wetting surfaces are referred to as hydrophilic and hydrophobic, respectively. If θ exceeds 150°, surfaces are designated superhydrophobic. However, on rough surfaces the measured contact angle often differs from the intrinsic one. This was first described by Wenzel in 1936 [Wen36], who implemented a roughness factor $r > 1$, which represents the ratio of the true surface area of the solid to its horizontal projection (Figure 1b). With this factor, the roughness dependent Wenzel contact angle θ^{W} can be calculated as follows:

$$cos\,\theta^{W} = r \cdot \cos\theta \quad (2)$$

Thus, Wenzel´s geometrical model allows explaining why the contact angle of hydrophilic surfaces decreases with increasing roughness whereas the contact angle of hydrophobic surfaces increases. However, Wenzel´s model can hardly explain water contact angles exceeding 150°. This behavior requires an additional model that was given by Cassie and Baxter in 1944 [Cas44]. Here, the surface tension γ dominates the system and it is energetically favourable for the liquid to form a droplet that rests on the tips of the surface while air fills the space between solid and liquid (Figure 1c). Consequently, only a small fraction of the surface φ_s is in contact to the liquid. The Cassie-Baxter contact angle θ^{CB} can then be calculated according to:

$$cos\,\theta^{CB} = \varphi_S \cdot \cos\theta + \varphi_S - 1 \quad (3)$$

According to Cassie-Baxter´s wetting state, water that is in contact to a superhydrophobic surface forms droplets that can easily unroll a surface at very low angles of inclination.
Thus, tailoring the surface roughness is an appropriate method to adjust the wettability of a material with a given contact angle θ. Beyond that, chemical surface modifications can be used to adjust the wettability. Here, a straightforward method is represented by the silanization of hydroxylated surfaces [Rat04]. The leaving groups of the silane (e.g. $–OCH_3$, $-OCH_2CH_3$, -Cl) react with the OH-groups of the surface by releasing CH_3OH, CH_2CH_3OH and HCl, respectively. Silanes with a polar functional group (e.g. –C=O, $-NH_3$) can be used to generate hydrophilic surfaces whereas silanes with a non-polar functional group (e.g. $–CF_3$, $-CH_3$) are suitable to create hydrophobic surfaces.

Electrowetting
The interfacial tension between a sessile water droplet and an electrode covered with a hydrophobic dielectric layer can be significantly modified when applying a voltage between the electrode and the droplet [Ber93, Qui01] (Figure 2). The dielectric layer then acts as a capacitor with a minimal flow of electric current at the solid-liquid interface. The resulting charge lowers the interfacial energy γ_{sl}. Consequently, the droplet spreads the surface and the contact angle θ decreases [Mug05].

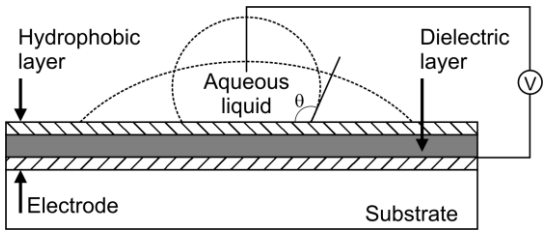

Figure 2: Principle of electrowetting on a dielectric material.

The relation between applied voltages and contact angle reduction can be derived from the Lippmann equation

$$\cos\theta_e = \cos\theta + \frac{\varepsilon_r \varepsilon_0}{2\gamma\, t}\, V^2 \tag{4}$$

where θ_e is the contact angle at the applied voltage V, ε_r and ε_0 is the dielectric constant of the dielectric and the permittivity of vacuum, respectively, and t is the thickness of the dielectric layer [Ber93].

Pyro- and piezoelectricity
The pyroelectric effect can be defined as a temperature-dependent polarization of the material that results in a change in the electrical flux density ΔD when the temperature T changes by ΔT [Lan74, Lan05]:

$$\Delta D = p \cdot \Delta T \tag{5}$$

The pyroelectric constant p is generally defined as the change in spontaneous polarization P_s with temperature T (at constant electric field E and constant mechanical stress σ):

$$p = \left(\frac{\partial P_S}{\partial T}\right)_{E,\sigma} \tag{6}$$

A necessary prerequisite for finding pyroelectric properties in solids is a spontaneous polarization of the crystal in a single polar axis [Kop89]. The elementary cells therefore have dipole moments even without a change in temperature, which, summed up over the entire crystal, generate an electric field. Usually, however, this does not appear externally, since the surface charges are compensated by free charge carriers from the environment [Kop89, Lan05]. Thus the electrical field is shielded even after the contacting of a measuring instrument and no current flows. The

polarization of the elementary cells only changes when the temperature of the solid changes, which in turn leads to a change in the macroscopic total polarization. This results in a current flow to balance the surface charges. In most pyroelectric solids, polarization decreases with temperature, resulting in a negative pyroelectric constant *p*.

For a complete consideration of the pyroelectric effect, the temperature-induced expansion of the solid must also be taken into account. Without this influence, the behavior is only described by the primary pyroelectric effect. Normally, however, (pyroelectric) materials expand as the temperature increases. Analogous to the piezoelectric effect described in the following, this size change in turn induces a dipole, which also generates an electric field when summed up over the entire crystal. This indirect influence of temperature on polarization is called the secondary pyroelectric effect p_{sec} [Bha80] and can be determined by the thermal expansion α, the tensor of elastic stiffness *c* and the piezoelectric constant *d* [Lan74, Bha80]:

$$p_{sec} = d \cdot c \cdot \alpha \tag{7}$$

However, not all pyroelectric materials are also ferroelectric. This would require that the electrical polarization can be reversed by a sufficiently large external electrical field, which is not possible if, for example, an electric breakdown prevents the reversal of the polarity before the necessary field strength is reached [Kop89].

The piezoelectric effect corresponds to a change in the electrical polarization caused by a mechanical elastic deformation [Kop89]. Several polar axes can also be present for this purpose, so that piezoelectric materials do not necessarily have to be pyroelectric or even ferroelectric. The (direct) piezoelectric effect was discovered as early as 1890 by Jacques and Pierre Curie. From a microscopic point of view, the charge centers of the elementary cell shift during deformation, resulting in an electrical dipole. By summing up each elementary cell in the crystal, an effective surface charge is produced and a macroscopically measurable electric field is formed. In this way, *D* can be described under the influence of a mechanical stress σ as

$$D = d \cdot \sigma + \varepsilon \cdot E \tag{8}$$

Conversely, piezoelectric materials deform when exposed to an electrical voltage, which is called the inverse piezoelectric effect.

Laser-induced periodic surface structures

Concerning the engineering of surfaces with tailored functional properties, ultra-short pulsed laser processing gained rapidly increasing attention in the past decades. In this context, the fabrication of laser-induced periodic surface structures (LIPSS) in a single-step, direct-writing process emerged as a flexible and versatile technique [Bon17a]. They were first observed by Birnbaum [Bir65] in 1965 during the irradiation of semiconductors with ruby laser pulses. Since then extensive research was carried out to investigate the formation mechanism of these structures. In the meanwhile, LIPSS have been identified as a universal phenomenon on all types of materials [Bon12] providing outstanding properties of the laser-structured surface such as wettability, optical performance, bioactivity, and tribology [Bon12, Mue16]. LIPSS fabrication has mainly been demonstrated on flat substrates and more recently also on the curved surface of carbon fibers whose curvature is in the order of the incident laser wavelength [Saj15, Kun18]. As a main advantage, the large variety of influencing parameters including wavelength λ, laser peak fluence *F*, number of pulses *N*, angle of incidence θ, and beam polarization, allows to control the specific properties of LIPSS such as their alignment and spatial period. As exemplarily shown in Figure 3, LIPSS are classified with regard to their spatial period Λ into high-spatial frequency LIPSS (HSFL) (Figure 3a) and low-spatial frequency LIPSS (LSFL) (Figure 3b). LSFL are characterized by a period Λ close to the initial laser wavelength λ for strong absorbing materials (metals, semiconductors) and close to λ/n for dielectrics, where *n* refers to the refractive index of the dielectric material [Bon17b, Gra17]. The alignment of LSFL predominantly occurs perpendicular

to the electric field (E-field) vector of the linearly polarized laser beam. Exceptions are related to some dielectric materials (e.g. fused silica, BaF_2) and certain polymers, where LSFL are aligned parallel to the laser beam polarization [Bon12, Reb13, Mez18]. It is well-accepted that the formation of LSFL can be explained by spatially modulated intensity pattern resulting from interference of the incident laser radiation with surface electromagnetic waves that are generated by scattering at the rough surface. This process might include the excitation of surface plasmon polaritons (SPP) and requires the consideration of surface roughness and isolated defects [Sip83, Gar11, Hua09]. An alternative approach to explain LIPSS formation is given by self-organization of the irradiated material [Gre16,Reb13]. HSFL are still controversially discussed in literature and a deep understanding of the formation mechanism is still missing. They have been observed solely for the irradiation with fs-laser pulses mainly on transparent materials, but also on metals with spatial periods much smaller than λ and an orientation both parallel as well as perpendicular to the linear beam polarization [Bon12]. Possible explanations include non-linear materials transport [Rei02], second-harmonic generation [Bor03], chemical surface alterations (e.g. oxidation) [Li14] and transient propagation effects in the laser-excited material [Rud17, Bul13].

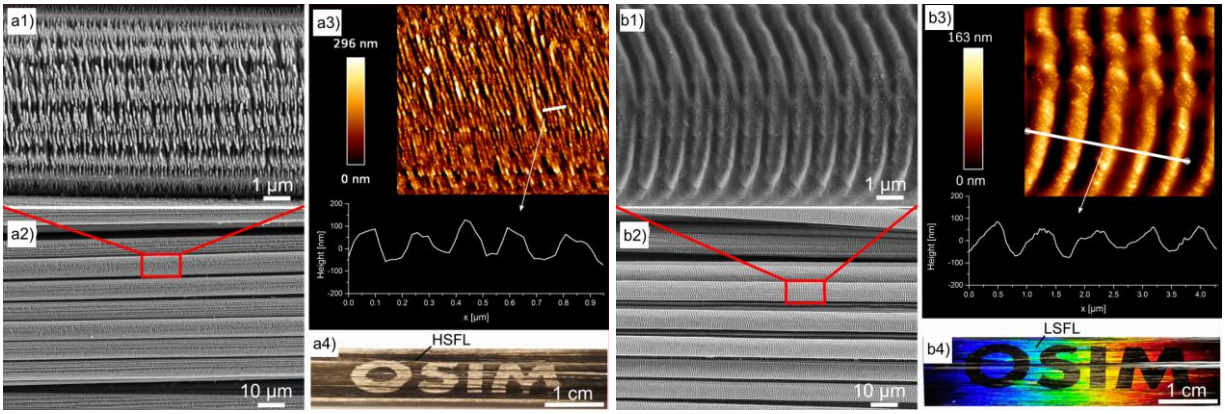

Figure 3: SEM micrographs, AFM micrographs and photographs of LIPSS on carbon fibers a) HSFL and b) LSFL [Kun18].

LIPSS formation was investigated in detail especially for metals [Rui14, Con15, Bon12, Bon14, Gra15, Gni17]. Regarding large surface areas with highly uniform LIPSS, Gnilitskyi et al. [Gni17] showed in experimental and theoretical investigations that specific metals such as steel, molybdenum, and titanium are promising candidates. As a main aspect, they observed a strong correlation between the LIPSS regularity and the $1/e^2$-decay length L_{SPP} of SPP (i.e. their mean free path) excited at the air-metal interface [Gni17]. Very regular grating structures can therefore be generated on metals with small values of L_{SPP}, i.e. on metals characterized by high optical damping. In contrast, large-area fabrication of LIPSS with reproducible properties on polymers by means of fs-laser radiation and a unidirectional scanning of the polymer surface remains a challenging problem [Mez18]. This is mainly caused by the strong non-linear absorption behavior of the material in the visible- and infrared wavelength range that is subject to permanent modifications during fs-laser-irradiation caused by intra- and inter-pulse effects (e.g. incubation) [Bon17b]. As an indirect LIPSS-based technique, the replica method allows to transfer the topography of fs-laser structured metal surfaces to polymeric materials. In this context, Liu et al. [Liu16] investigated the wettability of a structured stainless steel master, the resulting replica (polydimethylsiloxane) and of replicas sputtered with gold. They demonstrated a superhydrophobic behavior with self-cleaning effects on the PDMS replica. Based on a remarkable decrease of the contact angle related to the same replicas sputtered with a 300 nm thick gold layer (i.e. the sub-micro/nano-structures are eliminated), they confirmed the LIPSS-based surface structuring as the reason for the superhydrophobicity.

Preliminary work

Within the last ten years the work of Prof. Müller´s group focused on various laser-based techniques such as surface structuring, pulsed laser deposition (PLD), synthesis of nanoparticles by laser vaporization (LAVA), and selective laser sintering using mainly CO_2 and fs-laser systems as radiation sources. In terms of surface structuring, the irradiation with fs-laser pulses is a versatile and efficient method for the generation of nanostructured surfaces based on the formation of laser-induced periodic surface structures (LIPSS). These have great potential for applications in the fields of e.g., optics, power engineering and biomaterials. Using different substrate materials such as metals, semiconductors, dielectrics and composites, the development and properties of LIPSS as well as the properties of the material surfaces (e.g. optical properties, wettability) were investigated in dependence of laser beam and processing parameters (e.g. wavelength λ, pulse number *N*, laser peak fluence *F*, beam polarization, scanning speed). On stainless steel it was shown that the relationship between laser beam polarization and alignment of the resulting structures can be used to control the orientation of the LIPSS during the structuring process through the use of a continuously rotating *E*-field vector [**FM1**]. This allows transferring the originally well-ordered periodic ripples generated by a static linear polarization into surface morphologies with a precisely defined alignment and degree of disorder depending on the rotational frequency of the *E*-field vector. On glasses as the material of choice for numerous high-tech applications, the formation of LIPSS was evaluated as a function of the material properties caused by the different chemical composition of the examined glasses [**FM2**] and a preset surface temperature [**FM3**]. In this context, the different formation processes, the resulting spatial periods and the morphology were discussed based on the non-linear absorption behavior and the temperature-dependent viscosity. A study on metal-ceramic-composites showed that the surface of such materials can be selectively structured with LIPSS by exploiting their different light absorption behavior. This made it possible to adapt the wettability of the composite to the utilized laser fluence, opening up new approaches for biomedical and tribological applications [**FM4**].

Chemical surface functionalization has been the subject of numerous research studies in the past years. The aim was to enhance the *in vivo* osseointegration of titanium implants [**FM5**], to enhance the bonding potential of dental zirconia surfaces [**FM6**] and to enhance the mechanical properties of fiber-reinforced calcium phosphate cements [**FM7**]. Based on glass surfaces that were structured hierarchically with LIPSS, the fabrication of transparent samples with tailor-made wettability could be realized (Figure 4). The silanization of structured silica surfaces with trichloro(1H,1H,2H,2H-perfluorooctyl)silane allows to switch the wettability from superhydrophilic (θ = 0°) to superhydrophobic behavior with θ exceeding 150° [**FM8**].

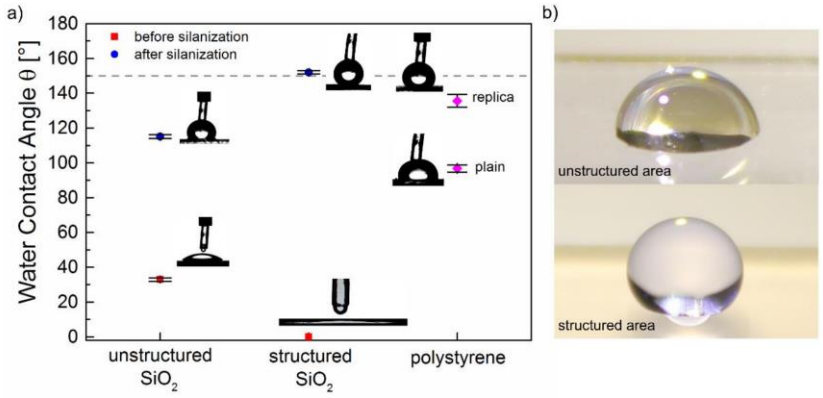

Figure 4: Analysis of the wettability of fused silica and polystyrene: (a) water contact angle θ of unstructured and structured fused silica before and after silanization in comparison to the contact angle of both surfaces that have been replicated by using polystyrene; (b) photographs of a water droplet illustrating the wettability of the unstructured and structured fused silica surface after silanization [FM8].

Due to the challenging problems concerning the direct-writing of large area LIPSS on elastomer surfaces, masters made of glass or stainless steel were successfully used in a replica casting process to transfer LIPSS and hierarchical surface structures to polystyrene and polyvinyl siloxane, respectively [**FM8, FM9**]. The polymer surfaces structured in this way show defined structural colors depending on their period, observation angle and illumination angle. During the elastic deformation of the structured elastomers, the increase in the LIPSS period leads to a color change towards colors with a larger wavelength (Figure 5).This mechano-responsive color change is reversible [**FM9**].

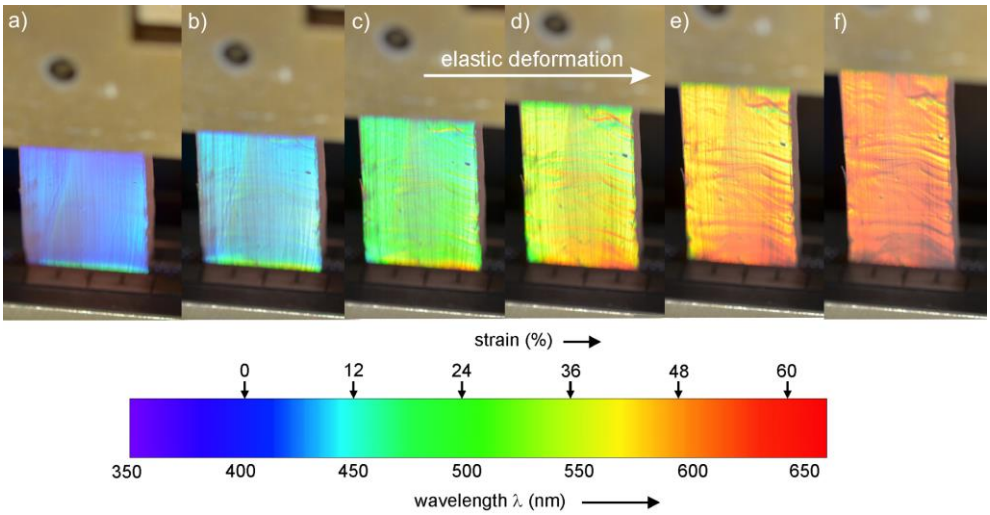

Figure 5: Structural colors resulting from LIPSS fabricated by replica casting using a stainless steel master. Elastic deformation with a total strain of (a) ε = 0%, (b) ε = 12%, (c) ε = 24%, (d) ε = 36%, (e) ε = 48%, and (f) ε = 60% results in a reversible mechano-responsive color-change in the visible electromagnetic spectrum from blue to red [FM9].

In the field of ferroelectric polymers, poly(vinylidene fluoride-co-trifluoroethylene) (P(VDF-TrFE)) was the subject of recent investigations [**FM10**]. P(VDF-TrFE) is a semicrystalline copolymer consisting of a ferroelectric crystalline β-phase embedded in an amorphous matrix. The β-phase has a quasi-hexagonal close packing with an orthorhombic *mm2* structure [Bun98]. This structure is responsible for the ferroelectric properties of the polymer and thus, in the polarized state, for its pyro- and piezoelectric properties. In our study, these ferroelectric properties of (Cd:Zn)S/P(VDF-TrFE) composite films were investigated with respect to the influence of the (Cd:Zn)S particle concentration and an additional photoexcitation of the composite material [**FM10**]. For both parameters, a strong influence on the ferro- and pyroelectric properties of the composite films was observed. For particle fractions that exhibit ferroelectric hysteresis, an increased remanent polarization and pyroelectric coefficient was obtained when a simultaneous optical excitation was applied.

1.1.1 Articles published by outlets with scientific quality assurance, book publications, and works accepted for publication but not yet published.

FM1 S Gräf, **FA Müller** „Polarization-dependent generation of fs-laser induced periodic surface structures” Appl. Surf. Sci. 331 (2015) 150-155.

FM2 S Gräf, C Kunz, **FA Müller** „Formation and properties of laser-induced periodic surface structures on different glasses” Materials 10 (2017) 933.

FM3 S Gräf, C Kunz, S Engel, TJY Derrien, **FA Müller** „Femtosecond laser-induced periodic surface structures on fused silica: The impact of the initial surface temperature” Materials 11 (2018) 1340.

FM4 C Kunz, JF Bartolome, E Gnecco, **FA Müller**, S Gräf „Selective generation of laser-induced periodic surface structures on Al_2O_3-ZrO_2-Nb composites" Appl. Surf. Sci. 434 (2018) 582-587.

FM5 C von Wilmowsky, L Müller, R Lutz, U Lohbauer, F Rupp, FW Neukam, E Nkenke, KA Schlegel, **FA Müller** „Osseointegration of chemically modified titanium surfaces: An in vivo study" Adv. Eng. Mater. 10 (2008) B61-B66.

FM6 U Lohbauer, M Zipperle, K Rischka, A Petschelt, **FA Müller** „Hydroxylation of dental zirconia surfaces: Characterization and bonding potential" J. Biomed. Mater. Res. B 87 (2008) 461-467.

FM7 AV Boehm, S Meininger, A Tesch, U Gbureck, **FA Müller** „Mechanical properties of biocompatible apatite bone cement reinforced with chemically activated carbon fibers" Materials 11 (2018) 192.

FM8 C Kunz, **FA Müller**, S Gräf „Multifunctional hierarchical surface structures by femtosecond laser processing" Materials 11 (2018) 789.

FM9 S Gräf, C Kunz, A Undisz, R Hanke, M Rettenmayr, **FA Müller** „Mechano-responsive colour change of laser-induced periodic surface structures" results not yet published.

FM10 S Engel, D Smykalla, B Ploss, S Gräf, **FA Müller** „Effect of (Cd:Zn)S particle concentration and photoexcitation on the electrical and ferroelectric properties of (Cd:Zn)S/P(VDF-TrFE) composite films" Polymers 9 (2017) 650.

1.1.2 Other publications

n/a

1.1.3 Patents

1.1.3.1 Pending

n/a

1.1.3.2 Issued

n/a

2 Objectives and work program

2.1 Anticipated total duration of the project

3 years starting 01.10.2019

2.2 Objectives

Our research proposal focuses on the dynamic wetting of flexible polymer substrates. For this purpose we will realize customized micro- and nanostructures on the surface of stretchable polymers. The wetting behavior will be controlled by surface functionalization and various external triggers.

The micro- and nanostructures are produced in the form of so-called laser-induced periodic surface structures (LIPSS) with the aid of an ultra-short pulsed fs-laser. The LIPSS formation process is based on interference effects in the focal spot between the incident laser beam and surface electromagnetic waves scattered at the rough surface. Selective ablation of the material leads to periodic structures that can be extended to large areas by scanning the laser beam over the substrate surface. LIPSS are characterized by their structural size in the order of the original laser wavelength and their specific orientation with respect to the laser beam polarization. Thus, the properties of the surface topography (structure size, alignment) can be precisely controlled by the laser beam parameters. However, the direct, large-area structuring of polymers with LIPSS represents a great challenge due to the strong non-linear coupling of the fs-laser radiation into

the material [Mez18]. Therefore, a homogeneous and reproducible structuring of large polymer surfaces, as required for wetting experiments and the dynamic wetting intended in the priority program, cannot be realized. In addition, studies on the irradiation of polymers with fs-laser radiation show that in some types of polymers the intensive fs-laser pulses can cause a laser-induced modification in the material structure (carbonization) and the chemical composition at the material surface (oxidation, formation of additional species) [Reb13]. The extent of this modification also depends on the wavelength of the laser radiation used and its intensity or fluence. Since the wetting behavior of the material surface is influenced significantly by its topography and chemistry, a systematic investigation of the wetting in dependence of external triggers would not be possible. Therefore, the present proposal aims on the structuring of metallic substrates, which have been demonstrated to be perfectly suitable for the fabrication of reproducible and highly regular LIPSS due to their linear absorption behavior at all available fs-laser wavelengths. In addition, the temporal control of the direction of the fs-laser beam polarization facilitates of generating surface structures with a well-defined alignment. Consequently, the tailor-made structured metal surfaces serve as masters, which can subsequently be used several times for the replica process and therefore allow a systematic investigation of the dynamic wetting of different polymer surfaces independent of their chemical composition.

After transferring the LIPSS topography from the metallic master to flexible and stretchable polymer specimens by a replica casting process we will pursue two different approaches to investigate the dynamic wetting:

i) Strain-dependent dynamic wetting of selectively functionalized nanostructured elastomers

In a first approach, hydrophilic and hydrophobic surface groups are coupled to the structured surface by a sequential method using hydroxylation, compression of the polymer surface and subsequent selective silanization with hydrophobic non-polar functional groups (Figure 6). In contact with water the prepared samples show superhydrophobic behavior due to roughness induced air pockets. Compression of the surface leads to a decrease in the contact angle until the smooth surface shows hydrophobic behavior. On the other hand, stretching the sample also reduces the contact angle as roughness is reduced and more and more hydrophilic functional groups come into contact with the water droplet. With continued stretching, the surface becomes hydrophilic due to the increasing specific amount of polar groups. In this way, the wettability of the polymer by mechanical deformation can be reversibly adjusted over a wide range.

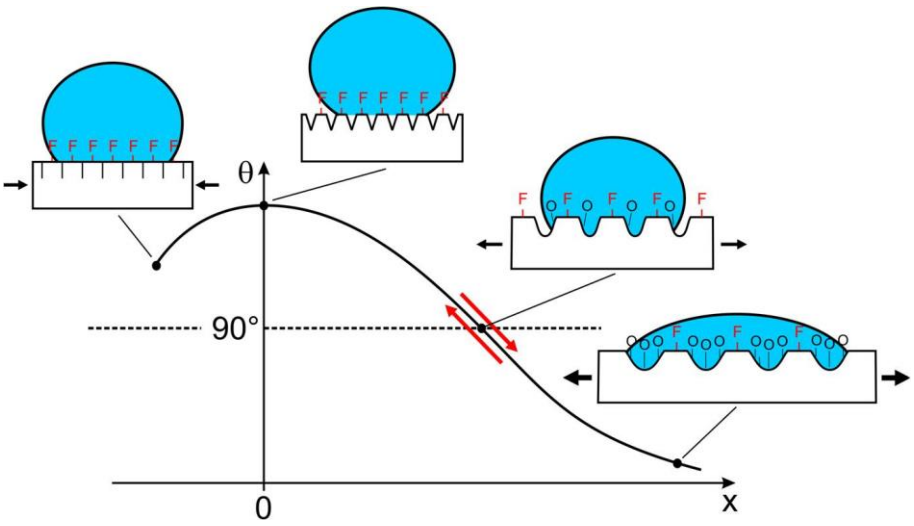

Figure 6: Functionalization of structured polymers.

ii) Dynamic electro-wetting of ferroelectric polymers as a function of temperature, deformation and voltage.

Our second approach is based on the so-called electro-wetting effect (Figure 2). Here, the contact angle can be controlled by an external voltage between the water droplet and the substrate. A dielectric layer between water and substrate prevents a current flow and leads to a permanent electric field. We intend to use polarized ferroelectric polymers or composites to generate the required electric field. These flexible ferroelectric substrates are polarized by corona polarization or polarization via metal electrodes that can be subsequently removed. Based on the pyro- or piezoelectric effect, the contact angle can be adjusted by temperature or mechanical stress as an external trigger (Figure 7). The starting point of the contact angle and thus the maximum working range is set by the LIPSS model, which is transferred to the polymer or composite surface by the replica casting process.

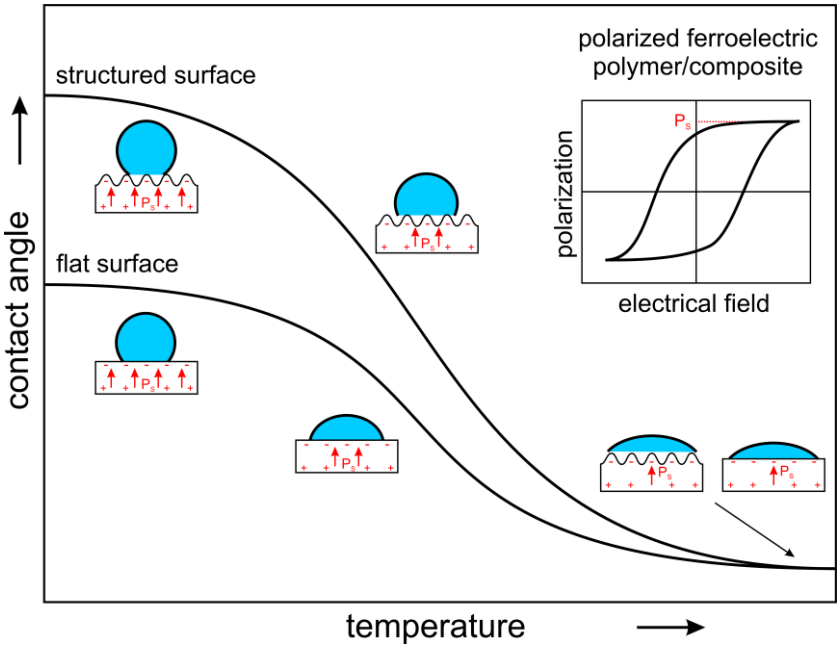

Figure 7: Pyro-electro wetting effect.

Contribution of the proposal to the generic, material-independent targets of the Priority Program

The present research proposal combines material synthesis aspects (laser processing, replica casting, and surface functionalization) with the mechano-responsive wetting of elastomers and the electro-, pyro-, and piezo-wetting of ferroelectric polymers. The applied experimental design allows to gain a deeper understanding of the fundamental mechanisms behind the dynamic (de)wetting of flexible, adaptive and switchable substrates and to design a new class of polymers that will be of particular interest for e.g. microfluidic and lab-on-a-chip devices. The elastomers used for the mechano-responsive wetting experiments in WP3 are highly flexible. The ferroelectric polymers used in WP4 are adaptive since the charge density of the polarized polymers changes in contact with water. Both types of materials are switchable by responding to an external trigger (e.g. mechanical deformation, voltage, temperature) and their substrate dynamics as well as wetting dynamics are reversible. For all experiments, water and water-based electrolytes are used as examples of well understood liquids. Our experimental data will be combined with numerical and theoretical contributions of collaborating groups to gain fundamental understanding of the dynamics of three-phase contact lines on nanostructured, flexible, adaptive and switchable polymer substrates. The scientific equipment and characterization facilities of the Otto-Schott Institute of Materials Research will be available to all partners of the Priority Program 2171. In

particular, our laser facilities are available to partners who are interested in integrating additional hierarchical levels of topography on their materials surfaces.

2.3 Work program incl. proposed research methods

WP1 LIPSS formation and production of metallic masters

The generation of highly uniform LIPSS will be investigated for different metallic substrate materials based on the results reported by Gnilitskyi et al. [Gni17]. The most promising candidates are stainless steel, titanium, molybdenum, and aluminum. For this purpose, samples with a size of (20x10) mm^2 are polished using suitable preparation methods to a surface average roughness of some nm (i.e. much smaller when compared to λ). After preparation, the samples will be ultrasonically cleaned (in ethanol and acetone for 10 min). The surface roughness will be measured using tactile profilometry (Form Talysurf 2, Taylor Hobson, England).

The ablation threshold and the threshold of LIPSS formation will be determined for the different types of metals by the irradiation of their surface in dependence on pulse energy E_{imp}, pulse number N, laser peak fluence F, pulse regime (pulse repetition frequency, equidistant pulses or laser bursts, accumulation effects), polarization state (static linear, dynamic polarization) and the available laser wavelengths of the utilized fs-laser (λ_1 = 1025 nm, λ_2 = 512 nm, and λ_3 = 342 nm) at normal incidence and air atmosphere using the experimental setup shown in Figure 8a. A generator for the second harmonic (SHG) is already available, a generator for the third harmonic (THG) is requested within this proposal. The variation of the angle of incidence of the laser beam at a fixed laser wavelength additionally allows to modify the LIPSS spatial period within a certain range and therefore provides an extension of the producible structure sizes. Evolution and properties of laser-induced surface structures are studied for the different wavelengths of the fs-laser using the previously determined parameter sets. Large areas with laser-induced surface structures are generated by means of a unidirectional scanning of the sample surface.

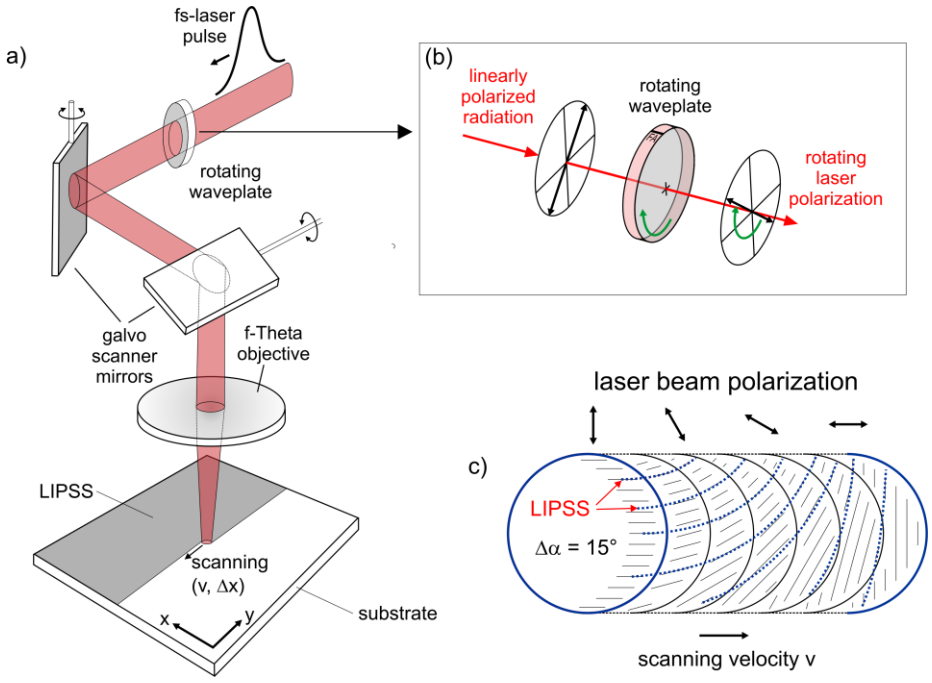

Figure 8: Formation of tailored LIPSS: a) Experimental setup, b) Dynamic polarization using a rotating waveplate and c) principle of LIPSS formation using a rotating E-field vector.

The relative movement is realized by a galvanometer scanner. In addition to the overlap Δy in scanning direction the influence of the overlap Δx and the direction of the E-field vector between

two adjacent lines on the resulting surface structures will be investigated. The resulting surface pattern induced by static linearly polarized radiation will be compared to the pattern obtained from a rotating laser polarization (Dynamic Polarization DP) (Figure 8b) in dependence on the rotation angle $\Delta\alpha$ of the E-field vector between two successive laser pulses (Figure 8c). $\Delta\alpha$ will be varied to investigate the influence of the DP on the disorder of the resulting surface structures. It has to be noted, that in addition to a continuous rotation of the E-field vector the rotation angle $\Delta\alpha$ can also be changed in an arbitrary manner relative to the scanning direction whereas the DP represents a powerful tool for the generation of versatile surface structures. The morphology of the LIPSS in terms of homogeneity, spatial period, modulation depth, and profile shape will be characterized by using white light interferometry, atomic force microscopy, and scanning electron microscopy in combination with Fast-Fourier-Transform analysis.

WP2 Replica casting

PDMS (polydimethyl siloxane) and PVS (polyvinyl siloxane) elastomers are used for the mechano-responsive wetting experiments. These polymers are widely used in dentistry [Sur13] and for microfluidic systems and biochips [Vla09] because of their ability to record accurate impressions and because they reproduce fine surface details. Beyond, they show excellent elastic recovery, adequate tear strength, and exceptional dimensional stability. Nanostructured PDMS and PVS replica surfaces will be fabricated by using a replica molding technique.

To prepare PDMS templates, a commercially available two-component siloxane polymer (e.g. Sylgard 184, Dow Corning) will be used. For this purpose, the vinyl-terminated prepolymer and the curing agent, which consists of a short hydrosilane crosslinker are mixed and the mixture is poured onto the patterned surface of the metallic master. The PDMS is cured at elevated temperatures (typically 60°C), and a solid but elastomeric polymer is formed. In the case of PVS, replica casting will be carried out with a commercially available two-component polymer (Mucopren®, Kettenbach, Germany). When the two components are mixed in the presence of a platinum salt catalyst (chloroplatinic acid), a reaction occurs between the silane and vinyl groups resulting in the crosslinking of a vinyl terminated polyvinyl siloxane. The polymer cures completely at room temperature after 30 min. After curing, PDMS and PVS replicas will be peeled off for further functionalization (see WP3).

P(VDF-TrFE) copolymers with different molar ratios of PTrFE to PVDF are used as ferroelectric polymers. However, copolymers with a PTrFE content of between 20 and 30% are mainly used, so that both the crystallization in the ß-phase occurs independent of pretreatment and the Curie temperature is above 100 °C (i.e. above the evaporation temperature of water). In this way, the maximum temperature range up to 100 °C can be used for the (electro-)wetting effect based on the pyroelectricity. Furthermore, different contact angles of the pure bulk polymers can be used, as well as different values for the remanent polarization or the dielectric constant. However, the targeted increase or variation of the contact angle is to be made possible primarily by the replica process. The impression of the previously generated LIPSS structures is made possible by two properties of the copolymer. On the one hand, P(VDF-TrFE) is soluble in various solvents (e.g. methyl ethyl ketone, diethyl carbonates, acetone), which enables the use of a spin coating process. On the other hand, P(VDF-TrFE) shows thermoplastic behavior, so that samples can also be produced by compression molding. The use of both processes enables a large and almost constant variation range of the sample thickness from the two-digit nm range up to several hundred µm. This is of particular interest with regard to polarization with instantaneous contact angle determination and pure (electro-)wetting based on an externally applied voltage (WP5). Thin samples in the nm to a few µm range are to be produced by spin coating, whereby the sample thickness is to be varied by the viscosity of the polymer solution, the rotational speed or multiple spin coating of individual layers. On the other hand, samples with a thickness in the single-digit to three-digit µm range can be produced using compression molding. In both processes, a metal foil structured with LIPSS serves as the master. The foils themselves are first

glued onto the carrier plate for spin coating and the stamp for compression molding. Subsequently, the LIPSS are generated according to the parameter space of the laser treatment specified in WP1. For spin coating, the metal foil simultaneously serves as a transfer foil in order to transfer the very thin samples undamaged onto a carrier substrate (e.g. ITO-coated glass) and then fix them there (e.g. glue them on). This has the advantage that the sample is not subjected to mechanical stress and, in the case of aluminum, for example, the carrier foil can be chemically dissolved by KOH without damaging the polymer sample itself or the surface structured with LIPSS. In this way, pure contact angle measurements as well as polarization investigations with simultaneous contact angle determination on the pure polymer surface can be carried out. The same applies to the (electro-)wetting investigations based on the pyroelectric or piezoelectric effect. Should a polarization of the ferroelectric polymer sample be necessary in advance, the metallic transfer foil can be used directly as an electrode or, after its removal, a specifically evaporated metal electrode (e.g. aluminum) can be used. The latter can also be chemically removed, e.g. by KOH. In the case of compression molding, the metal foil can be removed directly after the transfer of the sample to the carrier substrate, since the sample is mechanically more stable due to its greater thickness.

The morphology of replica casted polymer surfaces will be characterized in the same manner as the metallic masters in order to evaluate influences of the replica process on the topography (white light interferometry, atomic force microscopy, scanning electron microscopy in combination with Fast-Fourier-Transform analysis).

WP3 Strain dependent wetting

As a reference, contact angle measurements with water are made on cured PDMS and PVS samples with a smooth surface (Figure 9a). For this purpose, water droplets will be measured in the sessile drop mode (Krüss drop-shape analyzer 10 Mk2, Hamburg, Germany) with a minimum droplet volume of 2.5 µL.

In order to investigate the influence of surface roughness on the change in contact angle (equations 2 and 3), PDMS and PVS samples provided with LIPSS of different periodicity resulting from the fundamental laser wavelength and its 2nd and 3rd harmonic, respectively, are examined (Figure 9b). In order to investigate the influence of a reversible deformation of the polymer on the dynamic development of the contact angle, polymers equipped with LIPSS are elastically deformed by up to 100% perpendicular to the orientation of the LIPSS. This maximum deformation corresponds to a doubling of the LIPSS period of the respective sample. Here it has to be considered that due to the constant-volume condition during the deformation of a solid the depth of the LIPSS and consequently the roughness profile, which is important for the calculation of the wetting state, is changed. This is taken into account experimentally by roughness measurements in the stretched state utilizing white light interference microscopy. In the next step, the smooth polymers and those equipped with LIPSS are provided with polar groups to make them hydrophilic (Figure 9c). This is done by H_2O- and O_2-plasma functionalization (Diener Electronic Nano, Ebhausen, Germany) to achieve OH- and COO^--groups, respectively, and by wet chemical hydroxylation [God07]. Again, the contact angles are measured in the relaxed state and during elongation. Finally, hydroxylated samples are functionalized by silanization with e.g. a trichloro(1H,1H,2H,2H-perfluorooctyl)silane having non-polar hydrophobic functional groups (Figure 9d). For this purpose, the samples are placed in a desiccator close to a 100 µl drop of silane. Using a vacuum pump for 30 min, the silane will be deposited on the polymer surface by gas phase condensation [Kun18]. Then, the contact angles of silanized samples are investigated again in the initial and stretched state.

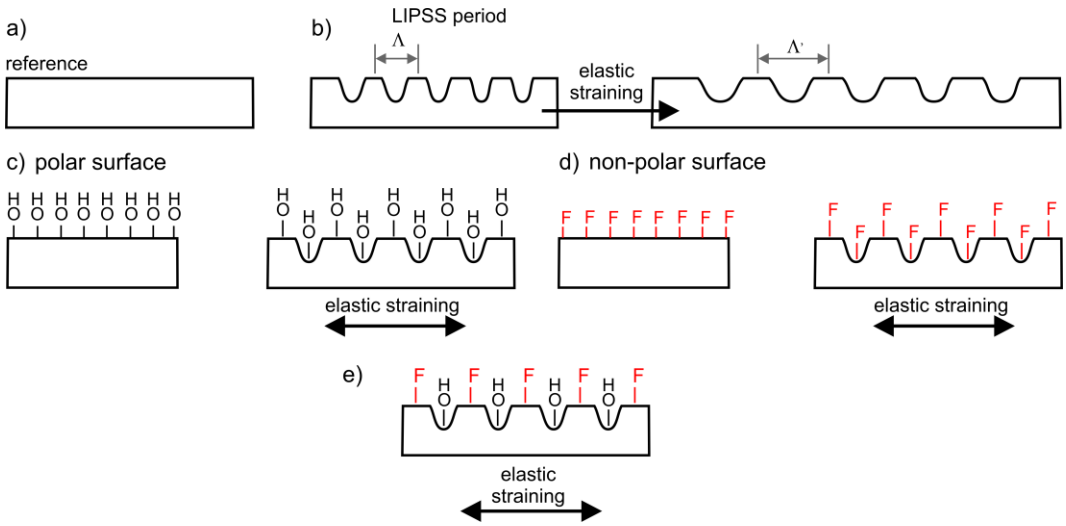

Figure 9: Schematic illustration of the experimental design in WP3.

In a final experiment, the hydroxylated samples are rolled towards the LIPSS to protect the polar groups in the LIPSS tip from atmospheric influences. In this state, the samples are silanized with trichloro(1H,1H,2H,2H-perfluorooctyl)silane and then rolled out so that hydrophilic and hydrophobic areas are present on the surface in periodic alternation (Figure 10). The contact angle of these samples is again measured in its initial state and the dynamic contact angle is recorded during stretching and relaxation (Figure 9e). Here it is postulated that the contact angle decreases with increasing elongation, since due to the decreasing height of the LIPSS, hydrophilic groups are increasingly involved in wetting, while the occupancy density of the hydrophobic groups decreases.

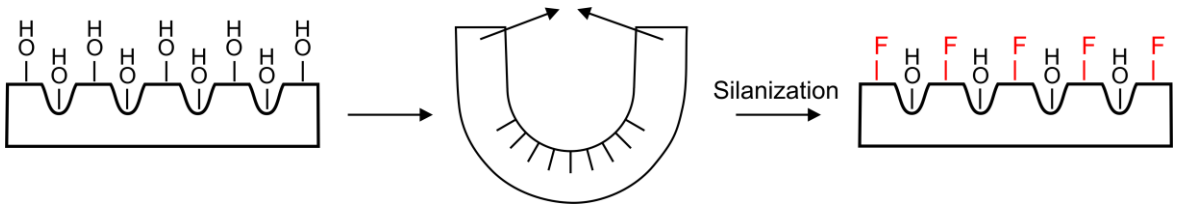

Figure 10: Preparation of nanostructured elastomer samples with periodically alternating hydrophilic and hydrophobic surface groups.

WP4 Electrowetting

The polymer films produced in WP2 have to be polarized in a first step. This can be achieved on the one hand by using the LIPSS-structured carrier film as electrode or an additionally vapor-deposited electrode (possibly even on both sides) with the aid of a Sawyer-Tower setup. This offers the advantage that the remanent polarization can be specifically adjusted to the electric field via the applied voltage (V to kV range) and thus taking the sample thickness into account. Subsequently, the metallic electrode must be chemically removed again (e.g. using KOH) so that the LIPSS remain on the surface, since the hydrophobic initial state, which is necessary for (electro-)wetting, can be adjusted in this way. Alternatively, the carrier film can be mechanically removed after transfer to the carrier substrate, especially in the case of thicker polymer samples produced by compression molding. Polarization can be carried out in advance by using a Sawyer-Tower setup, or subsequently by corona polarization, which makes an electrode superfluous by accelerating charge carriers (e.g. electrons) onto the sample and accumulating on the surface. The polarized samples are then tested for their (electro-) wetting properties based on the pyroelectric or piezoelectric effect (Figure 11a). On the one hand, the contact angle during heating or cooling of the sample is determined. Due to the pyrocoefficient *p* of the polarized polymer

sample, a temperature change leads to a change in the surface charge carrier density, which cannot be compensated. This change of the surface potential in turn results in a voltage or an electric field similar to electro-wetting, without an external voltage source. In this way, the contact angle should decrease with sufficient remanent polarization of the sample in combination with the temperature variation. A compensation of the pyroelectric potential by external charge carriers and thus a repeated increase of the contact angle is not excluded, but would have to be investigated by measurements over a longer period of time. Similar investigations are planned for the piezoelectrically driven (electro-)wetting effect. In particular, the d_{31} coefficient, i.e. the change in length of the sample perpendicular to the polarization direction, is to be exploited. However, such a tensile load perpendicular to the thickness of the specimen can also result in a change in the LIPSS period, provided that the tensile direction is also perpendicular to the orientation of the LIPSS. These influences must also be taken into account in addition to the different thicknesses of the sample. In particular, randomly orientated LIPSS generated with dynamic laser beam polarization (rotating *E*-field vector) (see WP1) will be of interest. Since the quantity of surface charges is independent of the thickness of the sample, the z-expansion should play a decisive role mainly during polarization. This also applies to the electro-wetting investigations, which are based on Kilaru and Heikenfeld [Kil07], who used a ferroelectric as dielectric. Here, the typical electro-wetting investigation of the contact angle as a function of external voltage is combined with ferroelectric polarization. These investigations are based on conventional electro-wetting investigations, whereby the water droplet itself acts as the electrode and thus a permanent change of the contact angle after the drop of the external voltage to zero should be observed due to the ferroelectric polarization (Figure 11b-d). In these measurements as well as in the investigations of the electrowetting based on the pyroelectric and piezoelectric effect, the influence of the pH-value and of dissolved ions (salts) will be evaluated. This is of particular interest with regard to their potential influence on surface charge, surface potential and electrostatically induced screening effects. Furthermore, the pyro- and piezoelectric influence shall be increased by increasing the degree of crystallinity (ß-phase) of the polymer. This is achieved by several annealing steps, which are accompanied by different characterization methods. In this way, FTIR and XRD are used to determine crystalline phases and the degree of crystallinity.

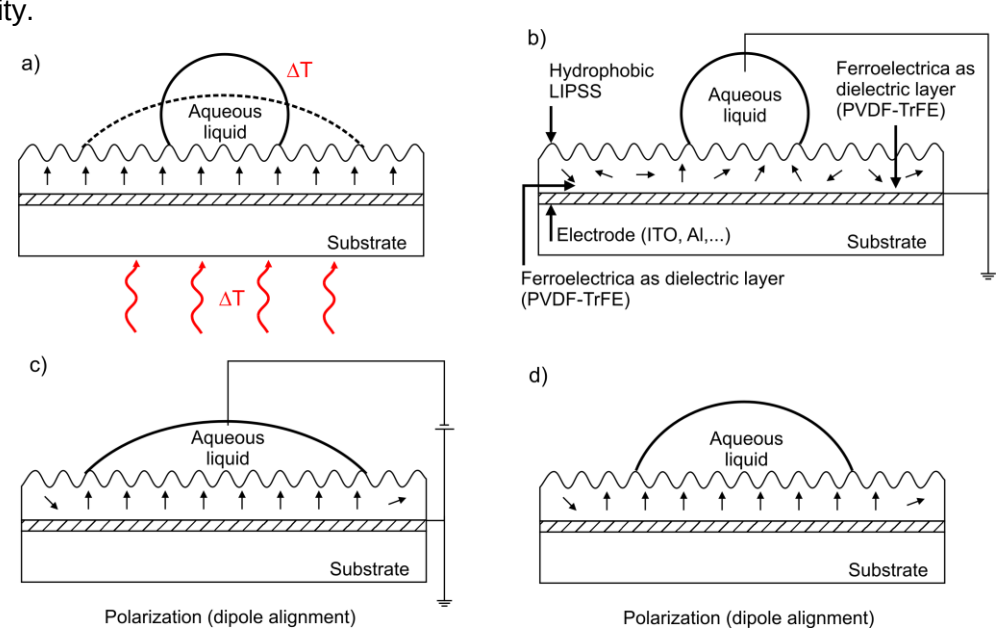

Figure 11: Schematic illustration of the contact angle of LIPSS-structured PVDF-TrFE films: a) pyroelectric wetting of a previously polarized sample that bases on the internal potential development during a temperature change, b) wetting without an applied voltage, c) electro-wetting with simultaneous polarization alignment by an applied voltage and d) wetting after polarization of the polymer without applied voltage.

2.4 Data handling

All research data produced during the project will be documented, stored and handled according to the rules of good scientific practice. The original electronic data will be stored on file systems of the university computing center and backed up on permanent storage devices (tape drive, DVD). Results from this project will be published in the appropriate scientific journals and books.

2.5 Other information

n/a

2.6 Descriptions of proposed investigations involving experiments on humans, human materials or animals as well as dual use research of concern

n/a

2.7 Information on scientific and financial involvement of international cooperation partners

n/a

2.8 Information on scientific cooperation within SPP 2171

Simulation:

- We are planning a close cooperation with the group of **Prof. Dr. Tatiana Gambaryan-Roisman (Darmstadt)**. Prof. Gambaryan-Roisman is interested in the simulation of drop propagation on deformable substrates with a given topography (as a precursor of a porous layer). With the help of our micro- and nanostructured polymer substrates, the model shall be validated experimentally and a parameter study shall be carried out on a large scale.
- The group around **Prof. Dr. Christian Holm (Stuttgart)** agreed to use their Lattice Boltzmann Electro Kinetics (LB-EK) model to study the dynamic wetting behavior of our nanostructured ferroelectric polymers as a function of solvent pH and an applied electric field.
- The group of **Dr. Michael Selzer (Karsruhe)** agreed to use our experimental data sets of strain-dependent wetting to perform phase field simulations of transport processes on the micro- and mesoscale.

Sample exchange:

- With the group of **Prof. Dr. Patrick Huber (Hamburg)**, who also deals with the topic of electrowetting, we have agreed to write LIPSS directly in silicon surfaces. Prof. Huber agreed to characterize the wetting of our ferroelectric polymers by high-resolution laser dilatometry.
- With the group around **Dr. Dorothea Helmer and Dr. Bastian Rapp (Karlsruhe)**, who are interested in integrating additional hierarchical levels of topography on their material surfaces, we have agreed to apply our replica casting process to their polymers. In addition, we will try to write small LIPSS areas directly into their nanoporous polymer surfaces without destroying their pore structure.
- It was agreed that LIPSS-structured metal masters will be made available to the groups of **Prof. Evgeny Gurevich and Prof. Jeanette Hussong (Bochum)**. They will be used to transfer the LIPSS-based nanostructures to magnetic nanocomposites by replica casting, whose lamellae angles and thus their wettability are controlled by a magnetic field.

Laser processing:

- In order to complement our experimental facilities with other fs-laser sources (shorter pulses, higher fluences, other wavelengths) intensive collaborations are planned with the research groups of **Prof. Evgeny Gurevich and Prof. Jeanette Hussong (Bochum)** and with the research groups of **Dr. Olga Varlamova and Dr. Rodica Borcia (Cottbus)**.

3 Bibliography

[Ber93] B Berge “Electrocapillarity and wetting of isolator films by water” Comptes Rendus de l´Academie des Sciences Serie II 317 (1993) 157-163.

[Bha80] A Bhalla, R Newnham “Primary and secondary pyroelectricity” Phys. Stat. Solidi A 58 (1980) K19-K24.

[Bir65] M Birnbaum “Semiconductor surface damage produced by ruby lasers” J. Appl. Phys. 36 (1965) 3688-3689.

[Bon12] J Bonse, J Krüger, S Höhm, A Rosenfeld “Femtosecond laser-induced periodic surface structures” J. Laser Appl. 24 (2012) 042006.

[Bon14] J Bonse, R Koter, M Hartelt, D Spaltmann, S Pentzien, S Höhm, A Rosenfeld, J Krüger “Femtosecond laser-induced periodic surface structures on steel and titanium alloy for tribological applications” Appl. Phys. A-Mater. Sci. Process. 117 (2014) 103-110.

[Bon17a] J Bonse, SV Kirner, S Höhm, N Epperlein, D Spaltmann, A Rosenfeld, J Krüger “Applications of laser-induced periodic surface structures (LIPSS)” Proc. SPIE 10092 (2017) 100920N.

[Bon17b] J Bonse, S Höhm, SV Kirner, A Rosenfeld, J Krüger “Laser-Induced Periodic Surface Structures – A Scientific Evergreen. IEEE J. Select. Top. Quant. Electron. 23 (2017) 9000615.

[Bor03] A Borowiec, HK Haugen “Subwavelength ripple formation on the surfaces of compound semiconductors irradiated with femtosecond laser pulses” Appl. Phys. Lett. 82 (2003) 4462-4464.

[Bul13] NM Bulgakova, VP Zhukov, YP Meshcheryakov “Theoretical treatments of ultrashort pulse laser processing of transparent materials: Toward understanding the volume nanograting formation and "quill" writing effect” Appl. Phys. B Lasers Opt. 113 (2013) 437-449.

[Bun98] AV Bune, VM Fridkin, S Ducharme, LM Blinov, SP Palto, AV Sorokin, SG Yudin, A Zlatkin “Two-dimensional ferroelectric films” Nature 391 (1998) 874-877.

[Cas44] ABD Cassie, S Baxter “Wettability of porous surfaces” Trans. Faraday Soc. 40 (1944) 546-551.

[Con15] J Cong, J Yang, B Zhao, X Xu “Fabricating subwavelength dot-matrix surface structures of Molybdenum by transient correlated actions of two-color femtosecond laser beams” Opt. Expr. 23 (2015) 5357-5367.

[Gar11] F Garrelie, JP Colombier, F Pigeon, S Tonchev, N Faure, M Bounhalli, S Reynaud, O Parriaux “Evidence of surface plasmon resonance in ultrafast laser-induced ripples” Opt. Express 19 (2011) 9035-9043.

[Gra15] S Gräf, FA Müller “Polarisation-dependent generation of fs-laser induced periodic surface structures” Appl. Surf. Sci. 331 (2015) 150-155.

[Gra17] S Gräf, C Kunz, FA Müller “Formation and Properties of Laser-Induced Periodic Surface Structures on Different Glasses” Materials 10 (2017) 933.

[Gre16] P Gregorcic, M Sedlacek, B Podgornik, J Reif “Formation of laser-induced periodic surface structures (LIPSS) on tool steel by multiple picosecond laser pulses of different polarizations” Appl. Surf. Sci. 387 (2016) 698-706.

[Gni17] I Gnilitskyi, TJY Derrien, Y Levy, NM Bulgakova, T Mocek, L Orazi “High-speed manufacturing of highly regular femtosecond laser-induced periodic surface structures: Physical origin of regularity” Sci. Rep. 7 (2017) 8485.

[God07] JM Goddard, JH Hotchkiss “Polymer surface modification for the attachment of bioactive compounds” Prog. Polym. Sci. 32 (2007) 698-725.

[Hua09] M Huang, FL Zhao, Y Cheng, NS Xu, ZZ Xu “Origin of laser-induced near-subwavelength ripples: Interference between surface plasmons and incident laser” ACS Nano 3 (2009) 4062-4070.

[Kil07] MK Kilaru, J Keikenfeld "Strong charge trapping and bistable electrowetting on nanocomposite fluoropolymer: Ba Ti O_3 dielectrics" Appl. Phys. Lett. 90 (2007) 212906.

[Kop89] K Kopitzki, P. Herzog “Einführung in die Festkörperphysik” (Springer, Berlin, 1989).

[Kun18] C Kunz, TN Büttner, B Naumann, AV Boehm, E Gnecco, J Bonse, C Neumann, ATurchanin, FA Müller, S Gräf “Large-area fabrication of low-and high-spatial-frequency laser-induced periodic surface structures on carbon fibers” Carbon 133 (2018) 176-185.

[Lan74] S Lang “Sourcebook of Pyroelectricity” (Gordon and Breach, New York, 1974).

[Lan05] SB Lang “Pyroelectricity: from ancient curiosity to modern imaging tool” Physics today 58 (2005) 31.

[Li14] XF Li, CY Zhang, H Li, Q-F Dai, S Lan, S-L Tie “Formation of 100-nm periodic structures on a titanium surface by exploiting the oxidation and third harmonic generation induced by femtosecond laser pulses” Opt. Express 22 (2014) 28086-28099.

[Liu16] B Liu, WJ Wang, GD Jiang, XS Mei, ZB Wang, KD Wang, JL Cui “Study on hierarchical structured PDMS for surface super-hydrophobicity using imprinting with ultrafast laser structured models” Appl. Surf. Sci. 364 (2016) 528-538.

[Mez18] M Mezera, M van Drongelen, GRBE Römer “Laser-Induced Periodic Surface Structures (LIPSS) on Polymers Processed with Picosecond Laser Pulses” JLMN 13 (2018) 105.

[Mue16] FA Müller, C Kunz, S Gräf “Bio-inspired functional surfaces based on laser-induced periodic surface structures” Materials 9 (2016) 476.

[Mug05] F Mugele, JC Baret “Electrowetting: From basics to applications” J. Phys. Condens. Matter 17 (2005) R704-R774.

[Qui01] C Quilliet, B Berge “Electrowetting: A recent outbreak” Curr. Opin. Colloidal Interface Sci. 6 (2001) 34-39.

[Rat04] BD Ratner, AS Hoffman, FJ Schoen, JE Lemons “Biomaterials Science – An Introduction to materials in medicine” (Elsevier Academic Press, San Diego, 2004).

[Reb13] E Rebollar, JR Vázquez de Aldana, I Martín-Fabiani, M Hernández, DR Rueda, TA Ezquerra, C Domingo, P Moreno, M Castillejo “Assessment of femtosecond laser induced periodic surface structures on polymer films” Phys. Chem. Chem. Phys. 15 (2013) 11287.

[Rei02] J Reif, F Costache, M Henyk, SV Pandelov “Ripples revisited: non-classical morphology at the bottom of femtosecond laser ablation craters in transparent dielectrics” Appl. Surf. Sci. 197-198 (2002) 891-895.

[Rud17] A Rudenko, JP Colombier, S Höhm, A Rosenfeld, J Krüger, J Bonse, TE Itina “Spontaneous periodic ordering on the surface and in the bulk of dielectrics irradiated by ultrafast laser: A shared electromagnetic origin” Sci. Rep. 7 (2017) 12306.

[Rui14] A Ruiz de la Cruz, R Lahoz, J Siegel, GF de la Fuente, J Solis “High speed inscription of uniform, large-area laser-induced periodic surface structures in Cr films using a high repetition rate fs-laser” Opt. Lett. 39 (2014) 2491.

[Saj15] R Sajzew, J Schröder, C Kunz, S Engel, FA Müller, S Gräf “Femtosecond laser-induced surface structures on carbon fibers” Opt. Lett. 40 (2015) 5734-5737.

[Sip83] JE Sipe, JF Young, JS Preston, HM Vandriel “Laser-induced periodic surface-structure.1. Theory” Phys. Rev. B 27 (1983) 1141-1154.

[Sur13] H Surapaneni, YP Samatha, YR Shankar, S Attili “Polyvinylsiloxanes in Dentistry: An Overview” Trends Biomater. Artif. Organs 27 (2013) 115-123.

[Vla09] ME Vlachopoulou, PS Petrou, SE Kakabakos, A Tserepi, K Beltsios, E Gogolides, “Effect of surface nanostructuring of PDMS on wetting properties, hydrophobic recovery and protein adsorption” Microelectr. Engin. 86 (2009) 1321-1324.

[Wen36] RN Wenzel “Resistance of solid surfaces to wetting by water” Chem. Res. 28 (1936) 988-994.

[You05] T Young “An essay on the cohesion of fluids” Philos. Trans. R. Soc. London 95 (1805) 65-87.

4 Requested modules/funds

4.1 Basic Module

4.1.1 Funding for Staff

Funding for a PhD student (E13, 75%) with a background in materials science, physics or chemistry is requested for three years. The PhD student will be responsible for the setup and operation of the experimental arrangement as well as the investigation of the dynamic (de)wetting on the different polymer surfaces. The comprehensive characterization of the surface properties will be performed using various methods including SEM, AFM, contact angle measurements, XRD, FTIR as well as the analysis of the surface topography by means of Fourier transformation.

4.1.2 Direct Project Costs

4.1.2.1 Equipment up to Euro 10,000, Software and Consumables

Equipment

- optical components for 3rd harmonic generation (THG) (crystals, mirrors, mounting parts) 9,500 €
- optical components for the UV wavelength range (extension of the consisting experimental setup requires additional beam splitters, mirrors and mounting parts) 3,000 €
- optics for control and analysis of beam polarization (waveplates, polarizer) 2,000 €
- focusing optics for the UV-wavelength range (aspheric lenses, F-Theta objective for the existing scanner system) 5,000 €
- accessories sputtering/evaporation system 1,000 €
- accessories/modification contact angle measuring device 1,000 €

Total: 21,500 €

Consumables

- raw sample materials (metals, polymers), preparation and handling 5,000 €
- ferroelectric polymer P(VDF-TrFE) 4,000 €
- service and maintenance of the fs-laser 5,000 €

Total: 14,000 €

4.1.2.2 Travel Expenses

Dissemination of the achievements as well as networking with colleagues of the SPP will be important for the key members of this proposal. Hence, the PI and the employed researcher will attend the SPP workshops in the 1st and 2nd year as well as an international conference (Europe) in the 2rd year in order to present the achieved results. Beyond the employed researcher will attend an Advanced School in the 1st year and a PhD candidate workshop in the 2nd year as well as an international conference (USA) in the 3nd year.

- SPP-related events 3,200 €
- International conference Europe (COLA 2021) 3,000 €
- International conference USA (MRS Fall Meeting Boston 2022) 3,000 €

Total: 9,200 €

4.1.2.3 Visiting Researchers

n/a

4.1.2.4 Expenses for Laboratory Animals

n/a

4.1.2.5 Other Costs

Contributions to running cost of equipment of other research groups at the FSU Jena

- Scanning electron microscope (DFG grant reference INST 275/241-1 FUGG) 2,500 €

Total: 2,500 €

4.1.2.6 Project-related publication expenses

750 € / year

Total: 2,250 €

4.1.3 Instrumentation

4.1.3.1 Equipment exceeding Euro 10,000

n/a

4.1.3.2 Major Instrumentation exceeding Euro 50,000

n/a

4.2 Module Temporary Position for Principle Investigator

n/a

4.3 Module Replacement Funding

n/a

4.4 Module Temporary Clinician Substitute

n/a

4.5 Module Mercator Fellows

n/a

4.6 Module Workshop Funding

n/a

4.7 Module Public Relations Funding

n/a

5 Project requirements

5.1 Employment status information

Prof. Dr. Frank A. Müller (Universitätsprofessor (W2), permanent position)

5.2 First-time proposal data

n/a

5.3 Composition of the project group,

Dr. rer. nat. Dipl.-Phys. Stephan Gräf (group leader laser, permanent university position)
Dipl.-Ing. Janet Grabow (technician, permanent university position)
Beyond, bachelor and master students preparing their thesis will be involved.

5.4 Cooperation with other researchers

5.4.1 Researchers with whom you have agreed to cooperate on this project

n/a

5.4.2 Researchers with whom you have collaborated scientifically within the past three years

Prof. Dr. K. Mandal (S. N. Bose National Centre for Basic Sciences, IND), Dr. J. F. Bartolome (CSIC-ICM Madrid, ESP), Prof. Dr. E. M. Farfan Torres (Universidad Nacional de Salta, ARG), Dr. A. Sanson (CNR-ISTEC Faenza, ITA), Dr. A. Smirnov (STANKIN Moscow, RUS), Prof. Dr. F. Belosi (University of Ferrara, ITA), Dr. E. Tyystjärvi (University of Turku, FIN), Dr. J. Méndez-Ramos (University La Laguna, ESP), Prof. Dr. Q. Y. Zhang (South China University of Technology, CHN), Prof. Dr. J. E. Barralet (Mc Gill University Montreal, CAN), Prof. Dr. J. Bonse (BAM Berlin, DEU), Prof. Dr. U. Gbureck (Universität Würzburg, DEU), Prof. Dr. B. Ploss (Ernst-Abbe-Hochschule Jena, DEU), Prof. Dr. J. Kiefer (Universität Bremen, DEU), Prof. Dr. C. Ronning (FSU Jena, DEU), Prof. Dr. J. R. Reichenbach (FSU Jena, DEU), Prof. Dr. E. Gnecco (FSU Jena, DEU), Prof. Dr. D. Fischer (FSU Jena, DEU), Prof. Dr. L. Wondraczek (FSU Jena, DEU), Dr. D. Kralisch (FSU Jena, DEU), Dr. U. C. Hipler (FSU Jena, DEU), Prof. Dr. C. Rüssel (FSU Jena, DEU), Prof. Dr. M. Kaluza (FSU Jena, DEU), Prof. Dr. B. Dietzek (FSU Jena, DEU), Prof. Dr. J. Popp (FSU Jena, DEU), Prof. Dr. A. Turchanin (FSU Jena, DEU), Prof. Dr. I. Hilger (FSU Jena, DEU)

5.5 Scientific equipment

The OSIM research facilities and its instrumentation are state of the art and include laboratories for materials synthesis and characterization. A particular strength of the OSIM is materials microscopy with light microscopy, polarized light microscopy, LSM, Raman microscopy, cryo-SEM, FIB-SEM, ESEM, TEM, and AFM. These facilities are complemented by XPS, FT-IR, XRD, GADDS, GDOES, contact angle measurement devices and versatile spectroscopic equipment including UV/VIS/NIR spectroscopy. A low-pressure plasma system is available at the CEEC Jena and can be used for the project. Beyond that, the group of Prof. Müller provides extensive equipment concerning several high power laser systems (Q-switched CO_2 laser, Yb:KYW thin disc fs-laser equipped with a generator for the second harmonic, fiber laser, diode laser, Nd:YAG laser, KrF excimer laser, HeCd laser) supplemented by different modulation techniques and comprehensive optical equipment for various laser processing techniques and the analysis of laser beam parameters.

5.6 Project-relevant cooperation with commercial enterprises

n/a

5.7 Project-relevant participation in commercial enterprises

n/a

6 Additional information

A request for funding this project has not been submitted to any other addressee. In the event that we submit such a request, we will inform the Deutsche Forschungsgemeinschaft immediately. In submitting a proposal for a research grant to the DFG, we agree to adhere to the DFG's rules of good scientific practice.